





Cite this: *Nanoscale*, 2020, **12**, 12046

A ligand-induced homojunction between aluminum-based superatomic clusters†

Dinesh Bista,^a Vikas Chauhan,^b Turbasu Sengupta,^a Arthur C. Reber ^a and Shiv N. Khanna ^{*a}

A superatomic molecule formed by joining two metallic clusters linked by an organometallic bridge can behave like a semiconductor and the addition of ligands can induce a significant energy level shift across an inter-cluster homojunction. This shift is induced by the *N*-ethyl-2-pyrrolidone ligands, and the placement of the ligands strongly affects the direction of the dipole moment, including the case where the dipole moment is parallel to the cluster interface. This computational study provides an alternative strategy for constructing nanometer-scale electronic interfaces between clusters mimicking semiconductor motifs. The semiconducting features in the PA_{12} clusters emerge from the grouping of the quantum states in a confined nearly free electron gas that creates a substantial energy gap. An organometallic $\text{Ge}(\text{CH}_3)_2(\text{CH}_2)_2$ bridge links the clusters while maintaining the cluster's electronic shell structure. The amount of level shifting between the bridged clusters can be changed by controlling the number of ligands. Attaching multiple ligands can result in a broken gap energy alignment in which the HOMO level of one cluster is aligned with the LUMO level of the other bridged cluster. Furthermore, the singly ligated bridged superatomic molecule is found to exhibit promising features to separate the electron-hole pairs for photovoltaic applications.

Received 1st April 2020,
Accepted 25th May 2020
DOI: 10.1039/d0nr02611e
rsc.li/nanoscale

1. Introduction

Band alignment at the interface of a diode takes place by stacking two semiconductor materials in bulk: a p-type semiconductor carrying an excess of holes and an n-type semiconductor with an excess of electrons.^{1–4} The difference in their chemical potentials causes diffusion of charge carriers that generate an internal electric field.^{5–10} Consequently, an in-built potential accompanied by an internal electric field at the interface results in a directional electrical current under an applied external bias voltage. Various kinds of p–n junctions in two dimensions have been proposed, for example, two 2D materials joined at the same plane provide the lateral junction while face to face stacking of materials leads to a vertical junction.^{11–13} An attractive alternative is electronics based on single molecules or clusters. Such systems exhibit valuable and unusual properties such as current rectification, photovoltaics, electronic switching, and negative differential resistance (NDR).^{14–25} The majority of such research has focused on molecular rather than cluster-based materials. In this work, we

investigate the possibilities of connecting simple metal clusters that attain closed electronic shells with large gaps and test the hypothesis that significant shifts in the level alignment across this ligand-induced homojunction may occur.

In this study, we link two metallic clusters with the open-electronic shell using an organometallic linker. Simple metallic clusters can have large HOMO–LUMO gaps because the quantum states in small symmetric clusters are bunched into electronic shells due to the quantum confinement.²⁶ The quantum confinement leads to quantum states with orbital character 1S, 1P, 1D... resembling the s, p, d... states in atoms, where the uppercase letters are used to denote states in clusters while the lower case letters are used for atoms.^{26–29} Research over the past thirty years has shown that the shell structure controls the electronic, magnetic, optical, and the chemical behavior.^{30–37} Extensive work has shown that the electronic structure of aluminum clusters can be fairly rationalized in terms of a confined nearly free electron gas.^{38–40} Aluminum is trivalent, so the PA_{12} cluster has a total of 41 valence electrons corresponding to a closed shell structure of $1\text{S}^2, 1\text{P}^6, 1\text{D}^{10}, 2\text{S}^2, 1\text{F}^{14}, 2\text{P}^6$ with an extra electron past the filled shell. Attachment of a bridging molecule to the PA_{12} cluster results in a covalent bond, which reduces the effective electron count to 40 valence electrons in the cluster maintaining a closed electronic shell with large HOMO–LUMO gap. Two PA_{12} clusters are joined by a $\text{Ge}(\text{CH}_2)_2(\text{CH}_3)_2$ linker, repre-

^aDepartment of Physics, Virginia Commonwealth University, Richmond, VA, 23284-2000, USA. E-mail: Snkhanna@vcu.edu

^bRamjas College, University of Delhi, Delhi-110007, India

†Electronic supplementary information (ESI) available. See DOI: 10.1039/d0nr02611e



senting an unsaturated version of a tetra-methyl germanium $\text{Ge}(\text{CH}_3)_4$, to form a bridged superatomic molecule, $\text{PAI}_{12}[\text{CH}_2\text{CH}_3\text{GeCH}_3\text{CH}_2]\text{PAI}_{12}$. We further show that such a bridged metallic cluster marked by a large gap, which can emulate semiconducting features arising from quantum confinement.

Generally, the chemical potentials of clusters are governed by the position of the HOMO and LUMO that in turn affects the electronic characteristics like the ionization energy and electron affinity. Recently, we have shown that the position of HOMO or LUMO in a variety of metal clusters can be tuned by using charge transfer ligands with electron-donating or accepting properties such as phosphine (PET_3 , PMe_3), CO, CN as they bond and form surface dipoles.^{41–50} We have also found that fused metal-chalcogenide clusters with unbalanced ligands may create intense internal electric fields that are ideal for separating electron-hole pairs in photon harvesting.⁵¹ In this work, we have induced a diode-like shift in the conduction and valence level group of states on both sides of the bridged superatomic molecule by attaching *N*-ethyl-2-pyrrolidone (EP = $\text{C}_6\text{H}_{11}\text{NO}$) ligands on one of the PAI_{12} clusters. We have previously shown that EP ligands raise the chemical potential of the cluster, making it an effective donor without changing the electronic shell structure.⁵² The proposed bridged superatomic molecule acts like a homojunction with a pronounced energy level shift and when enough ligands are added, the HOMO of the ligated cluster becomes aligned with the LUMO of the non-ligated cluster. This could be considered a cluster junction with a broken gap alignment. We note here that the junction has some unique properties, there is a pronounced shift in the energy levels across the junction, but both clusters are effectively intrinsic semiconductor with closed electronic shells. The energy level shift is due to the charge donating ligands and *via* the doping of the clusters. A unique feature of this arrangement is that the placement of the ligands primarily determines the direction of the dipole moment, so the net dipole moment may be parallel to the cluster interface. Independent of the placement of the ligands, a significant shift in the energy levels on both sides of the interface occurs. Finally, an examination of the optical spectra of our proposed bridged superatomic molecule reveals that the electrons and holes on each side of the inter-cluster interface are well-separated.

2. Results

2.1. Controlling the HOMO and LUMO *via* ligands

Our discussion starts with a brief review of how ligands can be used to modulate the position of energy levels. To show that the effect is general, we have investigated the effect of the EP ligand on the electronic states of Al_{13} and PAI_{12} clusters. Metallic clusters that have 40 valence electrons are found to have a closed electronic shell, hence, the Al_{13} cluster, with 39 valence electrons, can be regarded as a halogen superatom, while PAI_{12} cluster, with 41 valence electrons, behaves like an

alkali superatom. Fig. 1 shows the optimized ground-state structures of bare and EP ligated PAI_{12} and Al_{13} clusters and their corresponding one-electron energy. We find that the effective valence electron count or the electronic configuration of Al_{13} and PAI_{12} is not altered by the attachment of an EP ligand. For example, $\text{Al}_{13}(\text{EP})$ and Al_{13} are both one electron short of a closed electronic shell, with the last unfilled orbitals being 2P states (43 MO^{b} and 20 MO^{b}) leading to an open shell electronic configuration $1\text{S}^2, 1\text{P}^6, 1\text{D}^{10}, 2\text{S}^2, 1\text{F}^{14}, 2\text{P}^5$. ESI Fig. 1† represents the molecular orbital isosurface of the HOMO in Al_{13} and $\text{Al}_{13}(\text{EP})$. A similar phenomenon is observed in PAI_{12} and $\text{PAI}_{12}(\text{EP})$, both having one extra electron past the closed electronic shell, with the last filled orbitals in both clusters being 1G^1 . However, upon ligation, there is a pronounced upward shift in the entire electronic spectrum of Al_{13} and PAI_{12} , where the HOMO level of Al_{13} is raised from -5.10 to -4.47 eV (by 0.63 eV) while in case of PAI_{12} , HOMO level is raised from -3.72 to -3.13 eV (by 0.59 eV). ESI Fig. 2† depicts the molecular orbital isosurface of the HOMO in PAI_{12} and $\text{PAI}_{12}(\text{EP})$. For an open-shell system, the term HOMO implies the SOMO (Singly Occupied Molecular Orbital) level of the respective system. The raising of the electronic spectrum or chemical potential can be partly understood from the increased charge density in the core due to the electron-donating nature of the EP ligand. A Hirshfeld charge analysis confirms a gross charge of -0.369e^- and -0.349e^- on Al_{13} and PAI_{12} clusters respectively in the presence of EP ligand. The Hirshfeld charges, the values of the HOMO and LUMO levels, and the adiabatic ionization energy (AIE) for bare and ligated Al_{13} and PAI_{12} clusters are given in ESI Table 1.† The ligated clusters show the decrease in AIE relative to the bare clusters as the HOMO levels of the ligated clusters are raised in energy (see ESI Table 1†). One of the entities of our interest in the current work is the dipole moment of the ligated clusters due to local charge transfer. $\text{Al}_{13}(\text{EP})$ and $\text{PAI}_{12}(\text{EP})$ have dipole moments of 14.16 and 13.91 Debye respectively pointing from cluster to EP ligand, which confirms the donor nature of the ligand.

2.2. Superatomic clusters and Ge bridge ($\text{CH}_3\text{CH}_3\text{GeCH}_3\text{CH}_3$) molecule

To test our hypothesis that ligands may induce a significant shift in level alignment between two bridged metallic superatoms, we first need to identify a way for linking two metallic superatom clusters. An organometallic linker, tetramethyl germanium ($\text{Ge}(\text{CH}_3)_4$) is found to offer the possibility to connect two metallic superatomic clusters. This organometallic species has insulator like properties, with a very high HOMO–LUMO gap of 6.23 eV and AIE of 8.75 eV. It is noticed that the removal of one H atom from a CH_3 group leaves an unsaturated carbon, which binds the linker to the clusters through σ -bonding. The notation is made simpler by denoting $-\text{CH}_2\text{CH}_3\text{GeCH}_3\text{CH}_3$ linker as Ge^1_{B} , while Ge^2_{B} denotes the linker $-\text{CH}_2\text{CH}_3\text{GeCH}_3\text{CH}_2-$. The subscript 'B' represents that the Ge-linker is acting as a bridge between two clusters. Three metallic clusters, namely, MAI_{12} , ($\text{M} = \text{C}, \text{P}, \text{and Al}$) are chosen



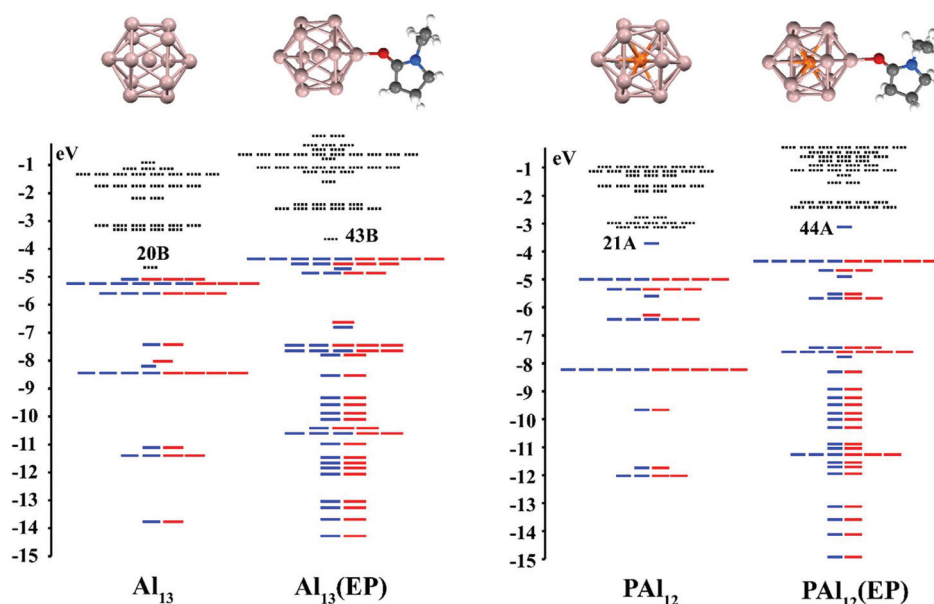


Fig. 1 One-electron energy levels of bare and EP ligated Al_{13} and PA_{12} clusters. Solid lines and dashed black lines represent the occupied and unoccupied energy levels respectively. The blue and red lines represent up and down spin states.

as possible motifs to form the bridged superatomic molecule with Ge-linker. The optimized geometric structures and electronic properties of $\text{MAL}_{12}\text{Ge}^1_{\text{B}}$ are given in ESI Fig. 3.† The $\text{CAL}_{12}\text{Ge}^1_{\text{B}}$ cluster turns out to be an open-shell system with a small HOMO–LUMO gap of 0.51 eV. $\text{Al}_{13}\text{Ge}^1_{\text{B}}$ is found to be a closed-shell system with a relatively high HOMO–LUMO gap of 1.45 eV. However, Al_{13} does not retain its icosahedron structure in the ground state of $\text{Al}_{13}\text{Ge}^1_{\text{B}}$. On the other hand, attaching Ge^1_{B} to PA_{12} cluster also results in a closed shell system with the highest HOMO–LUMO gap of 1.65 eV showing enhanced chemical stability among all the $\text{MAL}_{12}\text{Ge}^1_{\text{B}}$. Hence, the PA_{12} cluster is preferred as a suitable motif for building the bridged superatomic molecule. The binding energy (BE) is calculated using the following equation:

$$\text{BE} = E[\text{PA}_{12}] + E[\text{Ge}^1_{\text{B}}] - E[\text{PA}_{12}\text{Ge}^1_{\text{B}}] \quad (1)$$

where E is the total energy of the respective system. We have found that Ge^1_{B} strongly binds with the PA_{12} cluster with a BE of 2.85 eV. The PA_{12} cluster has 41 valence electrons, and the higher value of BE between the PA_{12} cluster and Ge^1_{B} is ascribed to the polar-covalent Al–C bonding that localizes one electron from the PA_{12} valence pool. Hence, PA_{12} attains a filled valence shell of 40 electrons leading to its electronic shell closure and a high HOMO–LUMO gap of 1.65 eV when bonding to the Ge-linker. To reveal its enhanced chemical stability, we performed the fragment analysis of $\text{PA}_{12}\text{Ge}^1_{\text{B}}$ as shown in Fig. 2. We found that LUMO of PA_{12}^+ (or HOMO of PA_{12}) hybridized with the HOMO of anionic Ge^1_{B} resulting in a stabilized bonding state forming the HOMO (−4.79 eV) of $\text{PA}_{12}\text{Ge}^1_{\text{B}}$, while the corresponding unoccupied anti-bonding states get higher in energy (MO = 42). Therefore, covalent bonding between Al and C leads results in a large gap of 1.65

eV. The Hirshfeld charge analysis of $\text{PA}_{12}[\text{Ge}^1_{\text{B}}]$, shown in ESI Table 2,† confirms that the C site of Ge^1_{B} binding with Al of PA_{12} acquires an extra charge of $\sim 0.09 e^-$ relative to charge on other C atoms in Ge^1_{B} .

2.3. Ge^2_{B} Bridged superatomic molecule $\text{PA}_{12}[\text{Ge}^2_{\text{B}}]\text{PA}_{12}$

After establishing that $\text{PA}_{12}[\text{Ge}^1_{\text{B}}]$ is a highly stable electronic system, we designed a bridged superatomic molecule in which two identical PA_{12} superatoms are bridged through an organo-metallic linker, Ge^2_{B} . Fig. 3 shows the optimized ground state structure of $\text{PA}_{12}[\text{Ge}^2_{\text{B}}]\text{PA}_{12}$. The bridged superatomic molecule turns out to have a large HOMO–LUMO gap of 1.53 eV. To see whether its electronic structure can be described by nearly free electrons gas, we have analyzed the molecular orbitals of $\text{PA}_{12}[\text{Ge}^2_{\text{B}}]\text{PA}_{12}$. Fig. 3 reveals a unique feature of the electronic structure of $\text{PA}_{12}[\text{Ge}^2_{\text{B}}]\text{PA}_{12}$ in which each PA_{12} cluster maintains its closed electronic shell structure with 40 valence electrons. It is important to highlight that this feature can be attributed to the presence of Ge-linker. We also find that Ge linker results in the splitting of 1D and 2P orbitals into bonding and anti-bonding pairs, and as a result, there are 12 delocalized 1D orbitals, constructed from 10 delocalized 1D orbitals and 2 molecular orbitals on the Ge, and 7 delocalized 2P orbitals constructed from 6 2P orbitals and 1 Ge molecular orbital. The bridged superatomic molecule has a relatively high AIE of 5.66 eV and a relatively low AEA of 2.16 eV.

In Fig. 4, we show the projected density of states of the bridged superatomic molecule corresponding to PA_{12} , Ge^2_{B} , and PA_{12} components as well as the one-electron energy levels of the bridged superatomic molecule. Interestingly, the HOMO of the bridged molecule is found to be −4.68 eV and each PA_{12} cluster is marked by a HOMO–LUMO gap of 1.53 eV. The



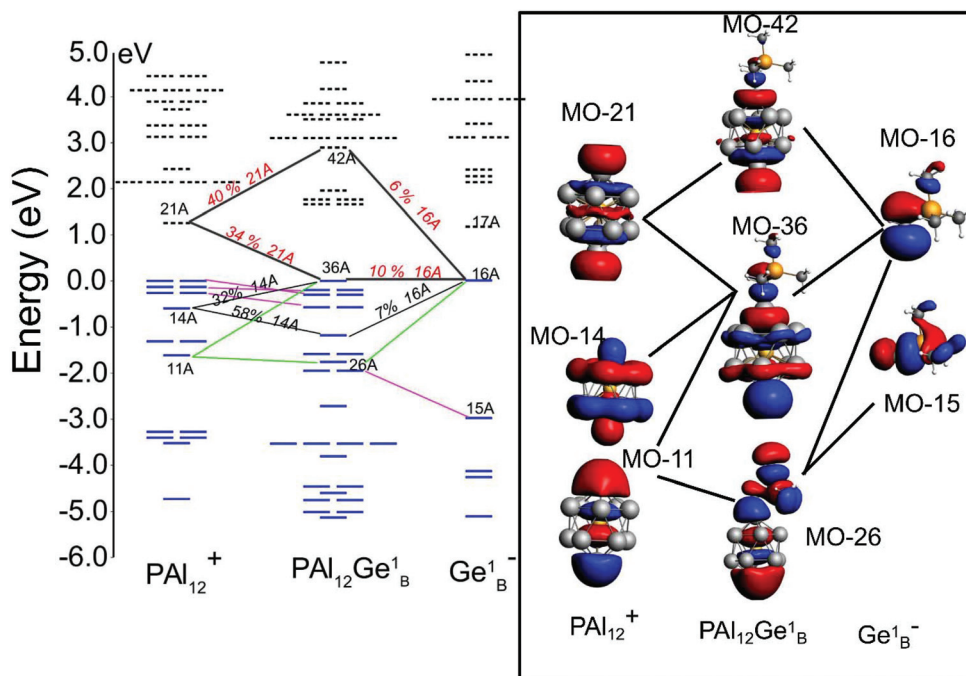


Fig. 2 Fragment analysis of $\text{PA}_{12}(\text{Ge}^1_{\text{B}})$ and isosurfaces of molecular orbitals.

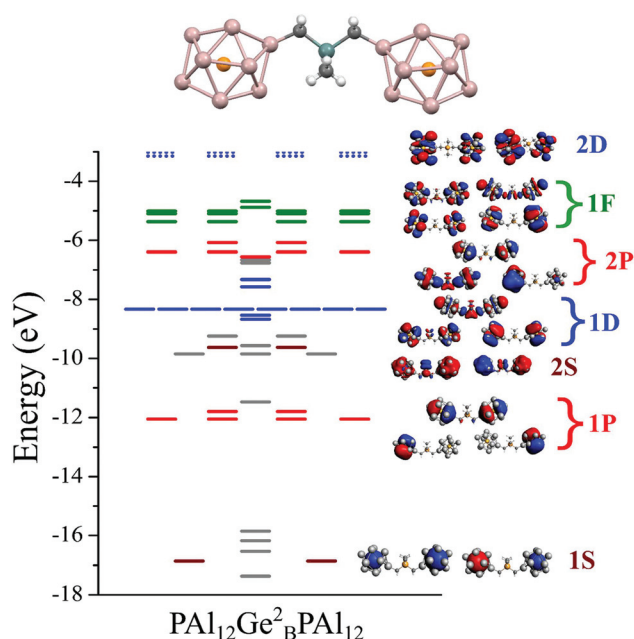


Fig. 3 Optimized ground-state structure and electronic structure of bridged superatomic molecule $\text{PA}_{12}[\text{Ge}^2_{\text{B}}]\text{PA}_{12}$. Solid and dashed lines represent the occupied and unoccupied energy levels respectively. The color-coding indicates the type of delocalized orbitals, and gray indicates orbitals localized on the Ge linker. Only a few delocalized molecular orbitals of P, D, and F characters are shown for clarity.

HOMO level is found to lower significantly compared with the bare PA_{12} (-3.72 eV), confirming that the bridged superatomic molecule no longer has alkali like superatomic behavior of bare PA_{12} cluster.

2.4. Effect of EP ligand on the electronic structure of the superatomic molecule

The basic premise of the current work is to demonstrate how a bridged superatomic molecule, consisting of two identical superatoms, can be transformed into an acceptor/donor pair with significant energy level shifts across the intercluster junction by changing the characteristics of one of the PA_{12} clusters. As we have discussed earlier that the addition of ligands can modulate the chemical potential of the clusters, we next examine whether that can also induce an internal electric field in our bridged superatomic molecule. We start with binding an EP ligand to one of the PA_{12} clusters to form $(\text{EP})\text{PA}_{12}\text{Ge}^2_{\text{B}}\text{PA}_{12}$ molecule. Fig. 5 shows the relative energy and structures of *ortho*, *meta*, and *para* $(\text{EP})\text{PA}_{12}\text{Ge}^2_{\text{B}}\text{PA}_{12}$. The assigning of *ortho*, *para*, and *meta* sites for attaching EP ligand is provided in ESI Fig. 4.† The *ortho*-isomer is found to be the most stable while *meta*- and *para*-isomers are 0.06 and 0.65 eV higher in energy respectively. The most stable configuration has the EP ligand pointing parallel to the inter-cluster interface. The *para* is relatively unstable because the binding of the organometallic linker has induced a charge donating active site on the opposite side of the cluster that reduces the binding of the charge donating EP ligand.^{53,54} We subsequently added two, three, and four EP ligands to form ligated $(\text{EP})_n\text{PA}_{12}\text{Ge}^2_{\text{B}}\text{PA}_{12}$ molecules as shown in Fig. 6A. The binding energies of the successive EP ligands are 0.91, 0.79, 0.56, and 0.32 eV respectively. The EP ligands bind to the aluminum sites of PA_{12} clusters through their oxygen atoms. While the binding energies are modest, there can be a significant effect on the electronic structure of the bridged superatomic clusters.



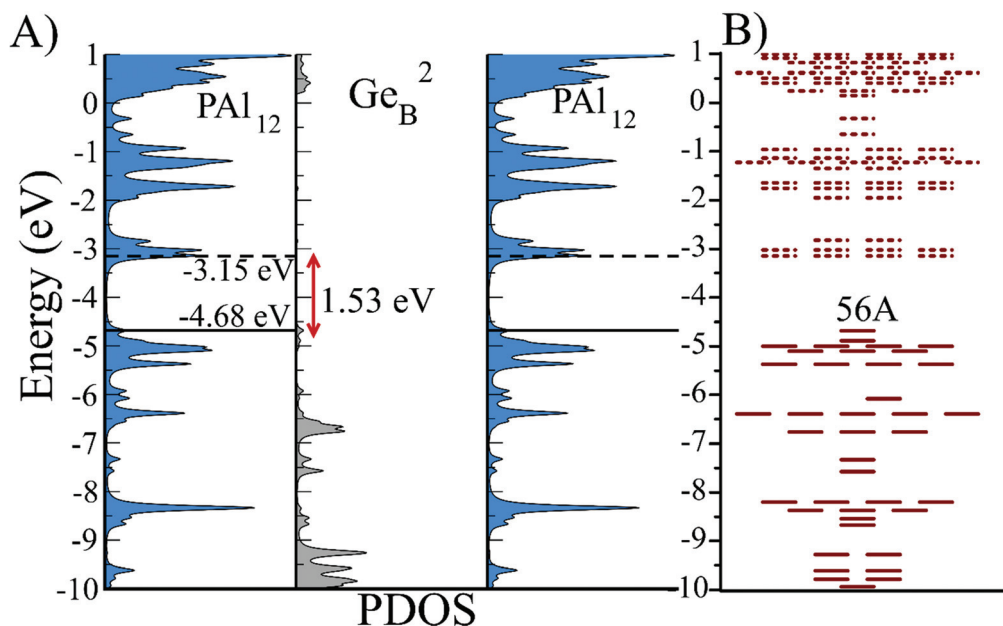


Fig. 4 (A) Partial density of states (PDOS) and (B) One-Electron energy levels of $\text{PAI}_{12}[\text{Ge}_2\text{B}]\text{PAI}_{12}$ molecule. Solid and dotted lines represent occupied and unoccupied levels respectively.

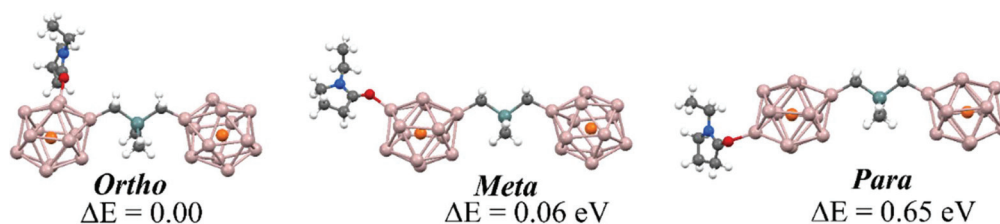


Fig. 5 Ground state structures of *ortho*, *meta*, and *para* isomers of $(\text{EP})\text{PAI}_{12}[\text{Ge}_2\text{B}]\text{PAI}_{12}$.

The addition of ligands changes the position of the HOMO indicating a shift in the chemical potential. Fig. 6B shows that the successive addition of four EP ligands raises the HOMO by 0.50, 0.58, 0.35, and 0.40 eV respectively from the previous size resulting in a total change of 1.83 eV. The electronic properties of the $(\text{EP})_n\text{PAI}_{12}\text{Ge}_2\text{BPAI}_{12}$, for $n = 1-4$, are given in Table 1. The rise in the HOMO is exclusively due to the orbitals that are located on the ligated cluster. The rise in HOMO leads to a monotonic decrease in the AIE, which decreases from 5.66 eV to 3.70 eV in going from zero to four ligands on the left PAI_{12} cluster ($\text{PAI}_{12}^{\text{L}}$). This is because higher is the HOMO, more easily a species can be ionized. However, the change in the AEA is not entirely monotonical as shown in Table 1.

The superatomic molecule with one ligand, $(\text{EP})\text{PAI}_{12}\text{Ge}_2\text{BPAI}_{12}$, is found to have a large dipole moment of 14.32 Debye, however, all this dipole is pointed from the cluster to the EP ligand, perpendicular to the molecular axis and parallel to the inter-cluster interface. In a standard p-n junction, the n-type side is positively charged, and the p-type side is negatively charged causing an internal dipole to point from p-type to n-type. Therefore, one would expect the dipole

to be pointed towards the ligated cluster. However, as seen in Table 1, the dipole along the supermolecular axis is merely -1.27 Debye, which represents the dipole pointing towards the ligated cluster. The strong electron-donating nature of EP is so dominating that almost all the dipole moment in $(\text{EP})\text{PAI}_{12}\text{Ge}_2\text{BPAI}_{12}$ points from the cluster to the EP ligand. Fig. 7 shows the magnitude and direction of dipole moment vectors in $(\text{EP})_n\text{PAI}_{12}\text{Ge}_2\text{BPAI}_{12}$ for $n = 1-4$. In the case with 2 and 3 EP ligands, the z-component of the dipole moment points backward, towards the “p-type” non-ligated cluster that should be negatively charged. The addition of the fourth EP ligand makes dipole moment perpendicular to the inter-cluster interface, dipole pointing from the non-ligated to the ligated side with a value of 8.55 Debye, out of a total dipole moment of 8.78 Debye. To determine if charge transfer is occurring across the cluster-cluster junction, we investigated the charging across the cluster as a function of the number of EP ligands.

In the ESI Table 3,[†] we show the net charge on the ligated side of the cluster monotonically increases from $+0.18e^-$, and reaches to $+0.23e^-$, $+0.26e^-$, $+0.29e^-$, and $+0.32e^-$, as the EP ligands are successively added. This confirms that the cluster



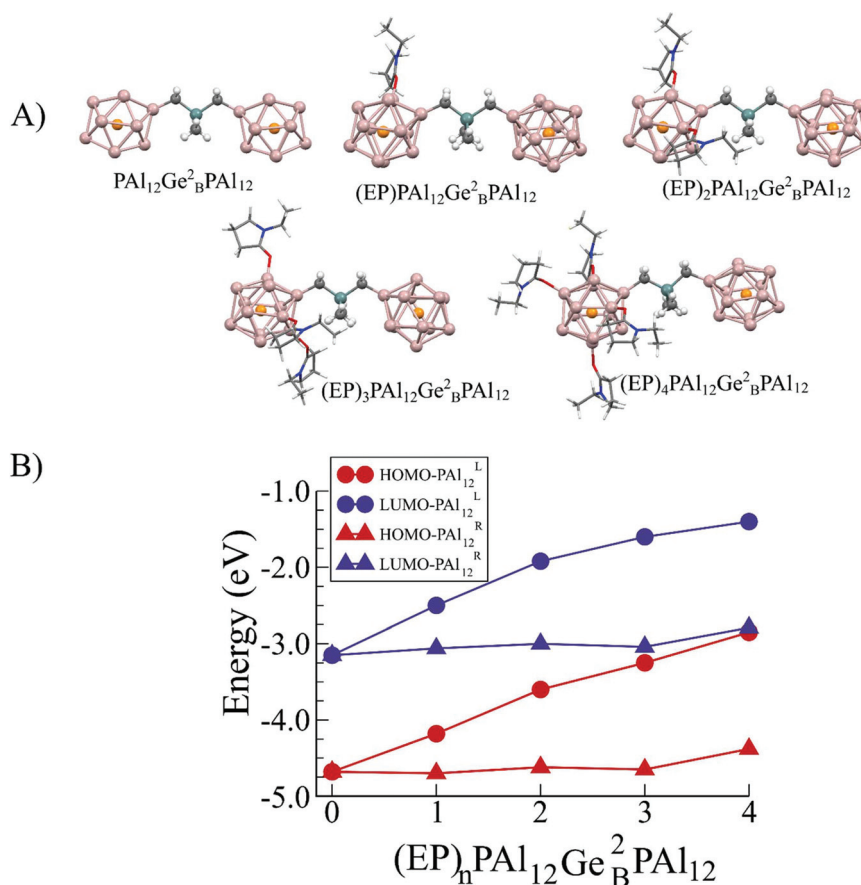


Fig. 6 (A) Ground state structures of $(\text{EP})_n\text{PAI}_{12}[\text{Ge}_2\text{B}]\text{PAI}_{12}$ for $n = 0-4$ and (B) HOMO–LUMO levels in left ($\text{PAI}_{12}^{\text{L}}$) and right ($\text{PAI}_{12}^{\text{R}}$) clusters of $(\text{EP})_n\text{PAI}_{12}\text{Ge}_2\text{BPAI}_{12}$ for $n = 0-4$ respectively.

Table 1 The electronic properties of $(\text{EP})_n\text{PAI}_{12}\text{Ge}_2\text{BPAI}_{12}$, for $n = 1-4$. The total dipole moment and their x -, y -, and z - components are also given in Debye

$(\text{EP})_n\text{PAI}_{12}\text{Ge}_2\text{BPAI}_{12}$	HOMO–LUMO gap (eV)	AIP	AEA	Dipole moment (Debye)	D_x	D_y	D_z
0	1.53	5.66	2.16	0.97	0.03	−0.97	0.00
1	1.13	5.21	2.43	14.37	−7.61	−12.13	−1.27
2	0.60	4.70	1.96	8.82	2.34	−8.28	1.93
3	0.21	4.19	2.13	5.62	0.91	−2.05	5.16
4	0.06	3.70	2.00	8.78	−1.45	1.36	−8.55

units are behaving like a p–n junction, however the direction of the net dipole is driven by the coordination of the ligand. Another interesting feature of the ligated bridged superatomic molecule is the decrease in the HOMO–LUMO gap, that decreases from 1.53 eV for the non-ligated system to 0.06 eV for the molecule with 4 ligands. As shown earlier, the addition of ligands changes the positions of HOMO and LUMO without significantly affecting the HOMO–LUMO gap,⁴³ and as shown in ESI Table S4,[†] however, our current result indicates a monotonic decrease in HOMO–LUMO gap with the gap almost disappearing when 4 ligands are attached to one side of the bridged superatomic molecule. Is there a contradiction?

To resolve this apparent paradox and to characterize the nature of the molecule, we now examine the electronic structure in more detail. We projected the density of states (DOS) of the ligand, the left cluster ($\text{PAI}_{12}^{\text{L}}$), bridge (Ge_2B), and the cluster on the right side ($\text{PAI}_{12}^{\text{R}}$). For the symmetric superatomic molecule without ligands, the PDOS on the left and right PAI_{12} is marked by a gap of 1.53 eV, as discussed earlier. The addition of a single ligand to the $\text{PAI}_{12}^{\text{L}}$ raises the HOMO and LUMO of the $\text{PAI}_{12}^{\text{L}}$ without any appreciable change in the HOMO–LUMO gap of the orbitals on that cluster ($\text{PAI}_{12}^{\text{L}}$). However, the LUMO of the $\text{PAI}_{12}^{\text{R}}$ becomes the effective LUMO of the combined system. This leads to an apparent decrease in



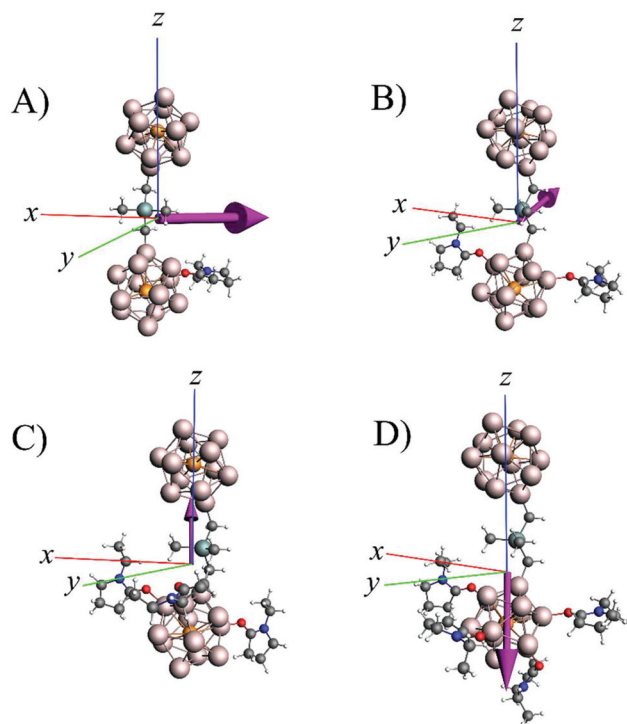


Fig. 7 The dipole moment vector in $(\text{EP})_n\text{PAI}_{12}[\text{Ge}_2\text{B}]\text{PAI}_{12}$ for $n = 1-4$ (A to D, respectively). The pink arrow represents the magnitude and direction of the total dipole moment vector. The origin of the cartesian-axes is taken at the center of mass of each system.

the HOMO–LUMO gap even though the PDOS on each side is marked by large HOMO–LUMO gaps. As seen in Fig. 8, for one EP ligand, the HOMO shifts up by 0.52 eV, and LUMO shifts up by 0.56 eV. With the successive addition of EP ligands, the shift of the HOMO increases to 1.02 eV, 1.40 eV, and 1.53 eV respectively. This process results in an apparent decrease in the HOMO–LUMO gap as the HOMO and LUMO are located at different clusters. More importantly, the combination now shows the PDOS on the $\text{PAI}_{12}^{\text{L}}$ is raised compared to the $\text{PAI}_{12}^{\text{R}}$, the hallmark of the p–n junction. One remarkable feature of the ligated bridged superatomic molecule with 3 and 4 EP ligands is that the HOMO of the ligated cluster becomes nearly aligned with the LUMO of the non-ligated cluster.

2.5. Electric field effects

To better understand the level alignment that is occurring across the inter-cluster interface, we have applied an external homogeneous electric field perpendicular to this interface. The z-axis of the superatomic molecule is aligned perpendicular to the interface, with the origin of cartesian co-ordinate placed at the center of mass of the whole molecule. The uniform external field is applied from the center of mass of the superatomic molecule along $\pm z$ -axes. This allows us to compare the effective level alignment induced by the ligands to the level alignment caused by the voltage drop due to the external homogeneous electric field. The effects of an external homogeneous electric field (in the negative z-direction) on the electronic states of $\text{PAI}_{12}[\text{Ge}_2\text{B}]\text{PAI}_{12}$ and $(\text{EP})\text{PAI}_{12}[\text{Ge}_2\text{B}]\text{PAI}_{12}$

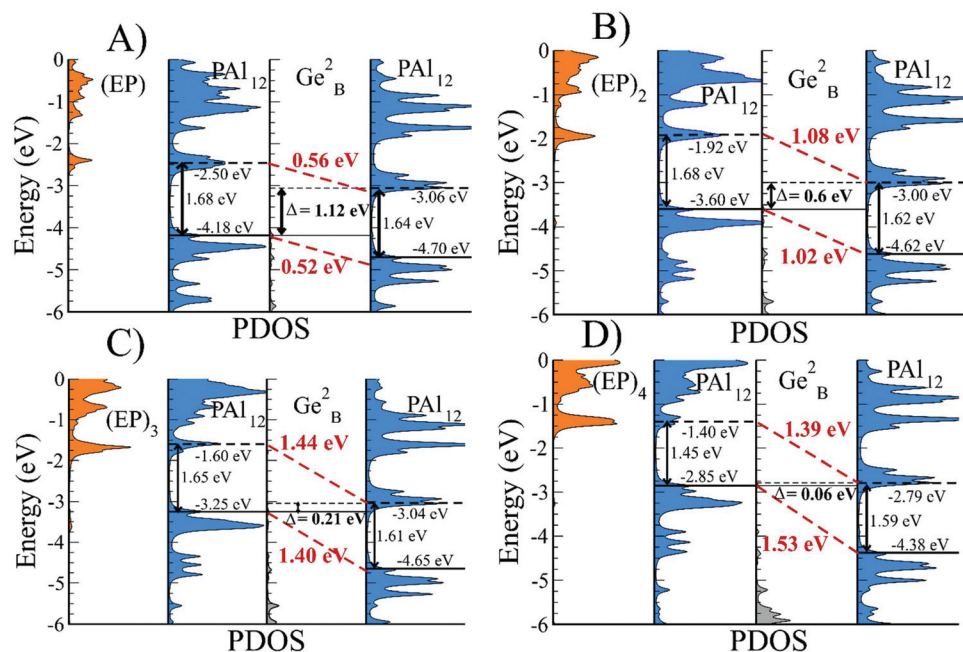


Fig. 8 The density of states of the $(\text{EP})_n\text{PAI}_{12}[\text{Ge}_2\text{B}]\text{PAI}_{12}$ for $n = 1-4$ (A to D, respectively). The projected density of states of both sides of the cluster are plotted separately with the ligated cluster on the left, and the non-ligated on the right. The red dotted lines indicate the shift of the HOMO and LUMO levels across the intercluster interface. HOMO–LUMO gaps in eV are given by Δ .



were examined *via* density of states and are shown in ESI Fig. 5 and 6.† The electric field results in a shift in the HOMO and LUMO levels on each side of the bridged superatomic molecule.

The shift is symmetric over both directions of the applied field for $\text{PAI}_{12}[\text{Ge}^2_{\text{B}}]\text{PAI}_{12}$ as shown in Fig. 9A. An electric field of -0.0036 a.u. (Hartree/e Bohr) results in a full level alignment in which the HOMO of $\text{PAI}_{12}^{\text{L}}$ aligns with the LUMO of the $\text{PAI}_{12}^{\text{R}}$. Likewise, 0.0036 a.u. aligns HOMO of the $\text{PAI}_{12}^{\text{R}}$ to the LUMO of the $\text{PAI}_{12}^{\text{L}}$. This corresponds to a voltage drop of about 3.2 V across the two PAI_{12} clusters to fully align the HOMO and LUMO. ESI Fig. 7† gives the PDOS of $\text{PAI}_{12}[\text{Ge}^2_{\text{B}}]\text{PAI}_{12}$ molecule in the presence of an applied homogenous electric field in positive z -axis. In the case of the ligated superatomic molecule, $(\text{EP})\text{PAI}_{12}[\text{Ge}^2_{\text{B}}]\text{PAI}_{12}$, we see that the levels are not aligned at the zero electric fields. An approximate electric field of 0.001 a.u. needs to be applied to align the HOMO of the left and right clusters. As shown in Fig. 9B, it requires an electric field of -0.0026 a.u., which corresponds to 2.3 V, to align HOMO of $\text{PAI}_{12}^{\text{L}}$ with LUMO of $\text{PAI}_{12}^{\text{R}}$. Hence, the effective voltage shift across the cluster due to the addition of a single EP ligand is about 0.9 V. Similarly, the HOMO of

$\text{PAI}_{12}^{\text{R}}$ can be also aligned with the LUMO of the ligated $\text{PAI}_{12}^{\text{L}}$ cluster. However, a larger (almost twice) electric field of $+0.005$ a.u., which correspond to voltages of 4.4 V, is required. These results confirm that the addition of the EP ligand produces an asymmetric bias in the response of the level alignment when a voltage is placed across the bridged superatomic molecule.

2.6. Optical absorption of $(\text{EP})\text{PAI}_{12}\text{Ge}^2_{\text{B}}\text{PAI}_{12}$

We now examine the potential of the bridged superatomic molecule to separate the electron-hole pairs for photovoltaic applications. Our earlier studies suggest that for a fused cluster to qualify for photovoltaics, the system should have following three attributes: (i) a large dipole moment to separate electron-hole pairs, (ii) The holes and electrons should be localized at different regions of the superatomic unit, and (iii) The optical gap must be greater than the HOMO–LUMO gap of the system, which would show that the electron-hole recombination is unlikely.⁵¹ The spin density of cationic and anionic states of $(\text{EP})\text{PAI}_{12}\text{Ge}^2_{\text{B}}\text{PAI}_{12}$ exhibit that the electron and holes are located at different regions of the bridged superatomic molecule as shown in Fig. 10A. The absorption spectrum of the molecule using time-dependent density functional theory

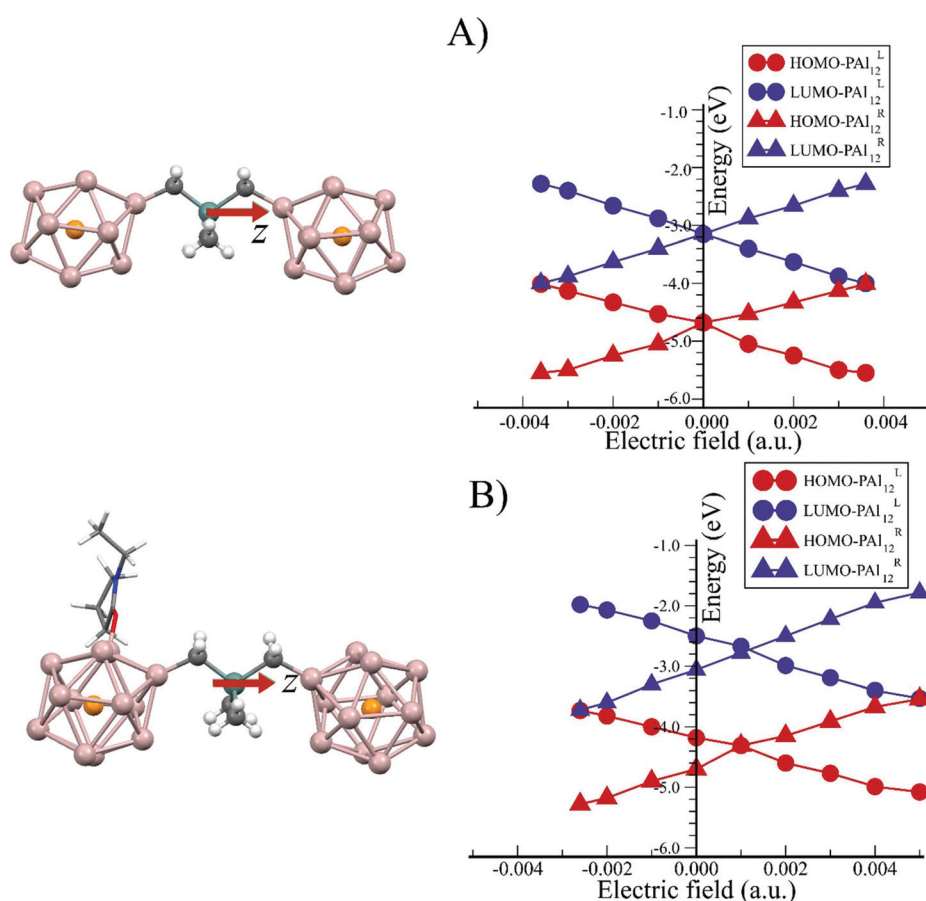


Fig. 9 (A) The energies of the HOMO and LUMO on the left and right cluster in $\text{PAI}_{12}(\text{Ge}^2_{\text{B}})\text{PAI}_{12}$ as a function of an electric field along the shown z -axis. (B) The energies of the HOMO and LUMO on the $\text{PAI}_{12}^{\text{L}}$ and $\text{PAI}_{12}^{\text{R}}$ clusters in $(\text{EP})\text{PAI}_{12}(\text{Ge}^2_{\text{B}})\text{PAI}_{12}$ as a function of an electric field along the shown z -axis.



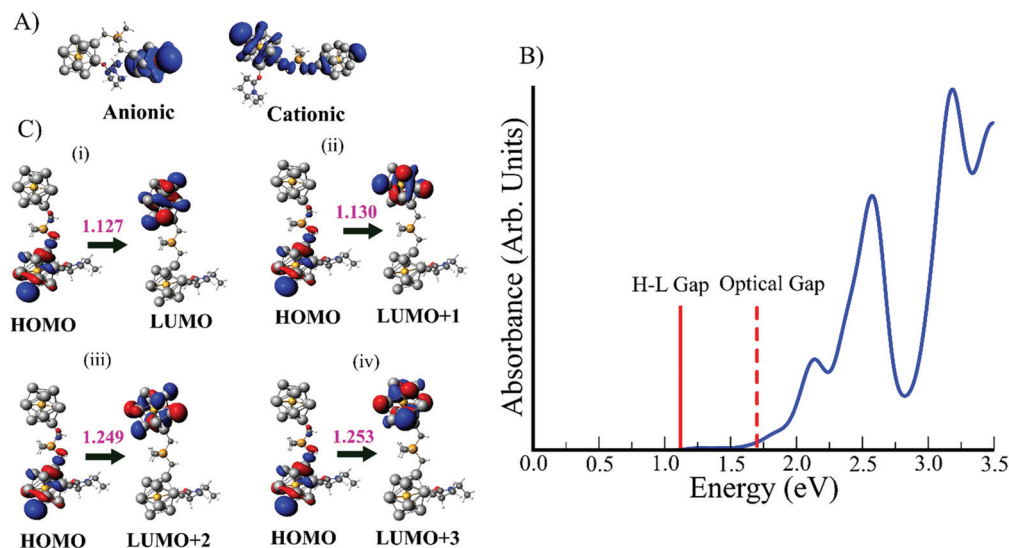


Fig. 10 (A) The spin density on the (EP)PAI₁₂Ge²⁺PAI₁₂ cluster to show the location of the electron and electron-hole. (B) The optical absorption spectra and (C) the orbitals corresponding to the low energy excitations that could cause electron-hole pair recombination. The excitation energies are given in eV and are represented in pink.

is also shown in Fig. 10B. This absorption spectra only considers allowed electric dipole transitions. The lowest energy excitation is 1.13 eV, however, as shown in ESI Table S5,[†] the oscillator strength for this excitation is very low, 7.0×10^{-7} . The effective optical gap is therefore around 1.70 eV. Transitions near the HOMO–LUMO gap turns out to have negligible oscillator strengths because the electron and hole are localized on different clusters. Fig. 10C displays the lowest four excitations: HOMO → LUMO, HOMO → LUMO+1, HOMO → LUMO+2, and HOMO → LUMO+3. In all of these cases, the holes are localized on the ligated PAI₁₂ part and the corresponding electron states are located on the non-ligated PAI₁₂ part of the molecule. These excitations are optically very weak leading to a low probability of electron-hole recombination *via* dipole allowed processes. Furthermore, since the electron and hole are well separated, this will also reduce non-radiative electron transfer, although we do not have a direct way of investigating this phenomenon. Our main purpose here is to show definitively that the electron and hole are well-separated by the ligand-induced junction. Hence, such a bridged metallic superatomic molecule can provide an alternative route to create separated electron-hole pairs for light harvesting.

3. Conclusions

The present studies show how the electronic states in metallic clusters associated with quantum confinement of a nearly free electron gas can have a well-defined HOMO–LUMO gap. The bridged superatomic molecule, PAI₁₂[Ge²⁺]_BPAI₁₂, is a possible model for such a device made out of metallic clusters. The Ge organometallic linker prevents the coalescing of the metallic clusters. The PAI₁₂ clusters have one more valence electron than a closed electronic shell, so by bonding with the linker,

the cluster attains a closed electronic shell. Hence, the germanium linker not only separates the individual clusters into two separate branches but also provides electronic stability. Once the clusters are stable and well separated, we can add ligands to alter the electronic structure. One of the unique features of the current proposal is how the addition of charge transfer ligands may alter the chemical potential of the individual clusters resulting in a junction with significant energy shifts. The addition of the EP ligand raises the levels of the cluster, on which the ligand is bound, leading to a shift in the alignment of levels across the inter-cluster junction. The dipole moment in such device is driven by the direction of the ligand-cluster bond, so the net dipole moment of the system can vary from parallel to perpendicular to the inter-cluster interface, depending on the direction of the bonding. The unit, (EP)PAI₁₂[Ge²⁺]_BPAI₁₂, is an intriguing system for photon harvesting, because the level alignment within the cluster may prevent the recombination of electron-hole pairs. These results reveal an alternative strategy for engineering internal electric fields across a cluster junction at the scale of a single nanometer.

4. Methods

4.1. Theoretical techniques

The studies performed here all used first-principles density functional methods using the Amsterdam Density Functional (ADF) program.⁵⁵ The exchange–correlation functional proposed by Perdew, Burke, and Ernzerhof (PBE) which uses the generalized gradient approximation (GGA) was used.⁵⁶ The TZ2P basis set was used with a large frozen electron core. The local minimum for each structure was found using the quasi-Newton method with no symmetry restriction and the lowest energy structures were ascertained. Relativistic effects were



incorporated using the zero-order regular approximation (ZORA).⁵⁷ We investigated several spin multiplicities to determine the most energetically stable ground state structure for the anionic, neutral and cationic species.

Author contributions

V.C and D.B conducted all the calculations. S.N.K, A.C.R., T.S., V.C, and D.B analyzed the results and the manuscript was written by S.N.K, A.C.R., V.C., and D.B.

Data availability

The structures, and data are given in the ESI.† All additional data generated or analyzed during this study are available via request to the corresponding author.

Conflicts of interest

The authors declare no competing interests.

Acknowledgements

The authors gratefully acknowledge funding by the US Air Force Office of Scientific Research (AFOSR), Grant No. FA 9550-18-1-0511.

References

- 1 Z. Zhang and J. T. Yates, *Chem. Rev.*, 2012, **112**, 5520–5551.
- 2 M. Alonso, R. Cimino and K. Horn, *Phys. Rev. Lett.*, 1990, **64**, 1947–1950.
- 3 M. Foussekis, J. D. McNamara, A. A. Baski and M. A. Reshchikov, *Appl. Phys. Lett.*, 2012, **101**, 082104.
- 4 A. C. Reber, S. N. Khanna, F. S. Roberts and S. L. Anderson, *J. Phys. Chem. C*, 2016, **120**, 2126–2138.
- 5 W. Shockley and H. J. Queisser, *J. Appl. Phys.*, 1961, **32**, 510–519.
- 6 L. M. Terman, *Solid-State Electron.*, 1962, **5**, 285–299.
- 7 S. J. Jiao, Z. Z. Zhang, Y. M. Lu, D. Z. Shen, B. Yao, J. Y. Zhang, B. H. Li, D. X. Zhao, X. W. Fan and Z. K. Tang, *Appl. Phys. Lett.*, 2006, **88**, 031911.
- 8 N. Yaacobi-Gross, M. Soreni-Harari, M. Zimin, S. Kababya, A. Schmidt and N. Tessler, *Nat. Mater.*, 2011, **10**, 974–979.
- 9 M.-Y. Li, Y. Shi, C.-C. Cheng, L.-S. Lu, Y.-C. Lin, H.-L. Tang, M.-L. Tsai, C.-W. Chu, K.-H. Wei, J.-H. He, W.-H. Chang, K. Suenaga and L.-J. Li, *Science*, 2015, **349**, 524–528.
- 10 Q. Kong, W. Lee, M. Lai, C. G. Bischak, G. Gao, A. B. Wong, T. Lei, Y. Yu, L.-W. Wang, N. S. Ginsberg and P. Yang, *Proc. Natl. Acad. Sci. U. S. A.*, 2018, **115**, 8889–8894.
- 11 M.-Y. Li, C.-H. Chen, Y. Shi and L.-J. Li, *Mater. Today*, 2016, **19**, 322–335.
- 12 Z. Zhang, P. Chen, X. Duan, K. Zang, J. Luo and X. Duan, *Science*, 2017, **357**, 788–792.
- 13 M. Mahjouri-Samani, M.-W. Lin, K. Wang, A. R. Lupini, J. Lee, L. Basile, A. Boulesbaa, C. M. Rouleau, A. A. Puztzky, I. N. Ivanov, K. Xiao, M. Yoon and D. B. Geohegan, *Nat. Commun.*, 2015, **6**, 1–6.
- 14 A. Aviram and M. A. Ratner, *Chem. Phys. Lett.*, 1974, **29**, 277–283.
- 15 P. Avouris, *Acc. Chem. Res.*, 2002, **35**, 1026–1034.
- 16 H. B. Akkerman, P. W. M. Blom, D. M. de Leeuw and B. de Boer, *Nature*, 2006, **441**, 69–72.
- 17 H. He, R. Pandey, J. U. Reveles, S. N. Khanna and S. P. Karna, *Appl. Phys. Lett.*, 2009, **95**, 192104.
- 18 H. He, R. Pandey, G. Mallick and S. P. Karna, *J. Phys. Chem. C*, 2009, **113**, 1575–1579.
- 19 X. Zhong, R. Pandey, A. R. Rocha and S. P. Karna, *J. Phys. Chem. Lett.*, 2010, **1**, 1584–1589.
- 20 L. Zhu and S. N. Khanna, *J. Chem. Phys.*, 2012, **137**, 164311.
- 21 L. Zhu, M. Qian and S. N. Khanna, *J. Chem. Phys.*, 2013, **139**, 064306.
- 22 B. Fu, M. A. Mosquera, G. C. Schatz, M. A. Ratner and L.-Y. Hsu, *Nano Lett.*, 2018, **18**, 5015–5023.
- 23 N. Xin, J. Guan, C. Zhou, X. Chen, C. Gu, Y. Li, M. A. Ratner, A. Nitzan, J. F. Stoddart and X. Guo, *Nat. Rev. Phys.*, 2019, **1**, 211–230.
- 24 B. M. Boardman, J. R. Widawsky, Y. S. Park, C. L. Schenck, L. Venkataraman, M. L. Steigerwald and C. Nuckolls, *J. Am. Chem. Soc.*, 2011, **133**, 8455–8457.
- 25 G. Lovat, B. Choi, D. W. Paley, M. L. Steigerwald, L. Venkataraman and X. Roy, *Nat. Nanotechnol.*, 2017, **12**, 1050–1054.
- 26 W. D. Knight, K. Clemenger, W. A. de Heer, W. A. Saunders, M. Y. Chou and M. L. Cohen, *Phys. Rev. Lett.*, 1984, **52**, 2141–2143.
- 27 S. N. Khanna and P. Jena, *Phys. Rev. B: Condens. Matter Phys.*, 1995, **51**, 13705–13716.
- 28 D. E. Bergeron, A. W. Castleman, T. Morisato and S. N. Khanna, *Science*, 2004, **304**, 84–87.
- 29 A. C. Reber and S. N. Khanna, *Acc. Chem. Res.*, 2017, **50**, 255–263.
- 30 D. E. Bergeron, P. J. Roach, A. W. Castleman, N. O. Jones and S. N. Khanna, *Science*, 2005, **307**, 231–235.
- 31 M. Walter, J. Akola, O. Lopez-Acevedo, P. D. Jadzinsky, G. Calero, C. J. Ackerson, R. L. Whetten, H. Grönbeck and H. Häkkinen, *Proc. Natl. Acad. Sci. U. S. A.*, 2008, **105**, 9157–9162.
- 32 P. Andre Clayborne, O. Lopez-Acevedo, R. L. Whetten, H. Grönbeck and H. Häkkinen, *J. Chem. Phys.*, 2011, **135**, 094701.
- 33 C. M. Aikens, *J. Phys. Chem. Lett.*, 2011, **2**, 99–104.
- 34 A. C. Reber, S. N. Khanna, P. J. Roach, W. H. Woodward and A. W. Castleman, *J. Am. Chem. Soc.*, 2007, **129**, 16098–16101.
- 35 Z. Luo, G. U. Gamboa, J. C. Smith, A. C. Reber, J. U. Reveles, S. N. Khanna and A. W. Castleman, *J. Am. Chem. Soc.*, 2012, **134**, 18973–18978.



- 36 G. U. Gamboa, A. C. Reber and S. N. Khanna, *New J. Chem.*, 2013, **37**, 3928–3935.
- 37 W. H. Blades, A. C. Reber, S. N. Khanna, L. López-Sosa, P. Calaminici and A. M. Köster, *J. Phys. Chem. A*, 2017, **121**, 2990–2999.
- 38 J. Akola, M. Manninen, H. Häkkinen, U. Landman, X. Li and L.-S. Wang, *Phys. Rev. B: Condens. Matter Mater. Phys.*, 2000, **62**, 13216–13228.
- 39 Z. Luo, C. J. Grover, A. C. Reber, S. N. Khanna and A. W. Castleman, *J. Am. Chem. Soc.*, 2013, **135**, 4307–4313.
- 40 J. C. Smith, A. C. Reber, S. N. Khanna and A. W. Castleman, *J. Phys. Chem. A*, 2014, **118**, 8485–8492.
- 41 T. C. Leung, C. L. Kao, W. S. Su, Y. J. Feng and C. T. Chan, *Phys. Rev. B: Condens. Matter Mater. Phys.*, 2003, **68**, 195408.
- 42 V. Chauhan, A. C. Reber and S. N. Khanna, *J. Phys. Chem. A*, 2016, **120**, 6644–6649.
- 43 A. C. Reber, V. Chauhan and S. N. Khanna, *J. Chem. Phys.*, 2017, **146**, 024302.
- 44 V. Chauhan, A. C. Reber and S. N. Khanna, *J. Am. Chem. Soc.*, 2017, **139**, 1871–1877.
- 45 V. Chauhan and S. N. Khanna, *J. Phys. Chem. A*, 2018, **122**, 6014–6020.
- 46 G. Liu, A. Pinkard, S. M. Ciborowski, V. Chauhan, Z. Zhu, A. P. Aydt, S. N. Khanna, X. Roy and K. H. Bowen, *Chem. Sci.*, 2019, **10**, 1760–1766.
- 47 A. C. Reber and S. N. Khanna, *npj Comput. Mater.*, 2018, **4**, 33.
- 48 Y. Yang, A. C. Reber, S. E. Gilliland, C. E. Castano, B. F. Gupton and S. N. Khanna, *J. Phys. Chem. C*, 2018, **122**, 25396–25403.
- 49 A. C. Reber, D. Bista, V. Chauhan and S. N. Khanna, *J. Phys. Chem. C*, 2019, **123**, 8983–8989.
- 50 G. Liu, V. Chauhan, A. P. Aydt, S. M. Ciborowski, A. Pinkard, Z. Zhu, X. Roy, S. N. Khanna and K. H. Bowen, *J. Phys. Chem. C*, 2019, **123**, 25121–25127.
- 51 A. C. Reber, V. Chauhan, D. Bista and S. N. Khanna, *Nanoscale*, 2020, **12**, 4736–4742.
- 52 V. Chauhan, A. C. Reber and S. N. Khanna, *Nat. Commun.*, 2018, **9**, 1–7.
- 53 Z. Luo, A. C. Reber, M. Jia, W. H. Blades, S. N. Khanna and A. W. Castleman, *Chem. Sci.*, 2016, **7**, 3067–3074.
- 54 M. B. Abreu, C. Powell, A. C. Reber and S. N. Khanna, *J. Am. Chem. Soc.*, 2012, **134**, 20507–20512.
- 55 G. te Velde, F. M. Bickelhaupt, E. J. Baerends, C. Fonseca Guerra, S. J. A. van Gisbergen, J. G. Snijders and T. Ziegler, *J. Comput. Chem.*, 2001, **22**, 931–967.
- 56 J. P. Perdew, K. Burke and M. Ernzerhof, *Phys. Rev. Lett.*, 1996, **77**, 3865–3868.
- 57 E. van Lenthe, J. G. Snijders and E. J. Baerends, *J. Chem. Phys.*, 1996, **105**, 6505–6516.

